Ultrathin High-Gain *D*-Band Transmitarray Based on a Spatial Filter Topology Utilizing Bonding Layer Effect

Dongyeon Seo, Hogyeom Kim, *Graduate Student Member, IEEE*, Seongwoog Oh, *Graduate Student Member, IEEE*, Jinhyun Kim, *Graduate Student Member, IEEE*, and Jungsuek Oh, *Senior Member, IEEE*

***Abstract*—This letter presents an ultrathin transmitarray (TA) in the *D*-band (110–170 GHz) by utilizing the bonding layer effect of spatial filters. The standard printed circuit board process limits the performance of spatial filters, resulting in a poor phase-shifting range in the sub-terahertz. The proposed unit cells based on the frequency selective surfaces use only two substrates to be ultrathin. By attaching the additional metal layer on the other side of the bonding substrate, the bonding layer effect can be maximized. Consequently, the proposed unit cells achieved a 271° phase-shifting range without any additional substrates. The proposed TA is the first to attain a high gain of more than 40 dBi in the *D*-band by reducing the quantization loss. The TA is synthesized using ten types of unit cells that have a low insertion loss of less than 1.5 dB. A 25.5 dBi horn antenna was selected as the source. The focal-to-diameter (*F*/*D*) ratio is 1.686 for the TA. The proposed TA, which is comprised of 50 176 elements, attains a peak gain of 44.3 dBi, an efficiency of 24.1%, and a bandwidth of 6% (134.5–143.5 GHz).**

***Index Terms*—Bonding layer effect, *D*-band, high gain, sub-THz, transmitarray (TA).**

I. Introduction

With the increasing popularity of wireless devices, data traffic has encountered a serious issue [1]. Large numbers of devices, including not only mobile phones but also the Internet of Things, use wireless communication due to its convenience. This situation causes a lack of bandwidth resources. In 6G communication, the Gbps data rate in the terahertz (THz) band, which is the frequency range from 0.1–10 THz, has been obtained [2]–[4]. However, the implementation of antennas in the THz band is challenging in terms of the inherent performance and rigorous communication environment, such as high loss, low fabrication precision, and high propagation loss in the free space [5], [6]. In particular, the attenuation due to atmosphere, rain-induced fading, and foliage cannot be neglected [7]–[9].

A transmitarray (TA) is an attractive candidate in terms of a high gain for overcoming high attenuation and its easy fabrication using the printed circuit board (PCB) process. The unit comprised of TA utilized spatial filters, bandpass filter, and low-pass filter, using frequency selective surfaces (FSSs) and can be a multilayer structure consisting of substrates, metal layers, and bonding layers [10]–[12]. The unit cells need to have the properties of low loss and a 360° phase-shifting range to obtain a high gain with reduced losses, which are insertion and quantization losses.

Stacking up more substrates of the unit cells enhances the phase-shifting range. When each substrate is laminated, the phase-shifting range is generally extended by 90°. However, increasing the number of substrates leads to a rise in insertion loss because the substrates are lossy.

In addition, it is not possible to completely align the position of the substrates when stacking in the PCB process. Furthermore, the fabrication error can often occur when laminating substrates in the PCB process. It does not make critical degeneration of the unit cell performance in the Ka-band. However, the wavelength in the THz band is short, so the fabrication error can cause the unit cell performance to be degraded. It is possible that laminating one more substrate might not help the phase-shifting range increase by 90°. As stacking more than three substrates in a PCB can cause fabrication errors, it is desirable to use one or two substrates for the unit cells in the sub-THz. The unit cells used two substrates that generally have a 180° phase-shifting range.

The bonding layer must be used to laminate substrates in the PCB process. The bonding layer in the Ka-band can be ignored because the thickness of the bonding layer is extremely thin compared with the wavelengths in the Ka-band. However, the bonding effect in the sub-THz cannot be negligible, so it must be considered when designing unit cells. The structure is called a doubled layer, which is the inserted metal layers to both sides of the bonding layer. It is called the bonding layer effect that considers the effect of the bonding layer using a doubled layer structure. The proposed unit cells use two substrates and one bonding layer using the doubled layer, maximizing the bonding layer effect to enhance the phase-shifting range with low insertion loss. The proposed unit cell achieved a 271.09° phase-shifting range without any additional substrates.

Manuscript received 29 April 2022; revised 10 June 2022; accepted 15 June 2022. Date of publication 28 June 2022; date of current version 6 October 2022. This work was supported in part by the Institute of Information and Communications Technology Planning and Evaluation Grant funded by the Korea Government (MSIT) under Grant 2019-0-00056 (Development of 3-D high accuracy motion recognition SoC for automobile applications based on 140 GHz electromagnetic waves) and in part by the Institute of Information and Communications Technology Planning and Evaluation Grant funded by the Korea Government (MSIT) under Grant 2021-0-00763 (Innovative Fusion Technologies of Intelligent Antenna Material/Structure/Network for THz 6G). (*Corresponding author: Jungsuek Oh.*)

The authors are with the Institute of New Media and Communications, Department of Electrical and Computer Engineering, Seoul National University, Seoul 08826, South Korea (e-mail: skaty15@snu.ac.kr; ghrua2424@snu.ac.kr; dillon1859@snu.ac.kr; jinhyun111@snu.ac.kr; jungsuek@snu.ac.kr).

Digital Object Identifier 10.1109/LAWP.2022.3186686

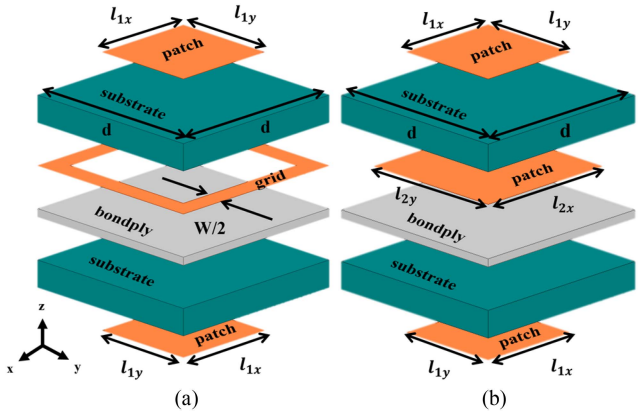

Fig. 1. Geometry of the conventional unit cell employing FSSs. (a) Bandpass filter type. (b) Low-pass filter type.

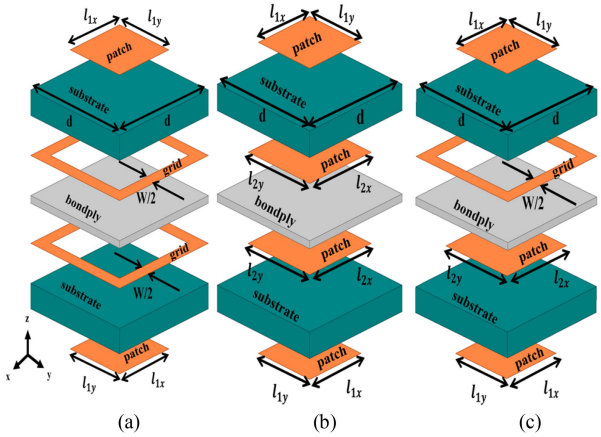

Fig. 2. Geometry of the proposed unit cell using FSSs. (a) Bandpass filter type. (b) Low-pass filter type. (c) Mixed filter type.

This letter proposes a low-profile TA with high gain by utilizing spatial filters. The proposed TA laminated with only two substrates has been thinly fabricated by the standard PCB process. The rest of this letter is organized as follows. Section II presents the novel unit cell configuration utilizing the bonding layer effect, which uses the doubled layer, and compares it to a conventional unit cell. Section III describes the simulation and measurement results obtained using the fabricated TA. Finally, Section IV concludes this letter.

II. Unit Cell Design

Fig. 1(a) and (b) shows the conventional types of unit cells laminated with two substrates, which are the bandpass and low-pass types. While the bandpass filter unit cell with three metal layers consists of two patches and a grid, the low-pass filter unit cell is composed of only three patches [13]–[15].

The proposed TA is composed of a square set of unit cells that have phase shifting. Each unit cell has a size ($d \times d$) of 0.9×0.9 mm^2 ($0.42\,\lambda_0 \times 0.42\,\lambda_0$), where λ_0 is the wavelength in the free space at 140 GHz. The periodicity of the unit cell is 0.9 mm. To synthesize accurate spatial filter responses, the proposed unit cells are utilized with FSSs. The geometries of the unit cells are presented in Fig. 2. All the unit cells are multilayer structures consisting of two dielectric substrates and four metal

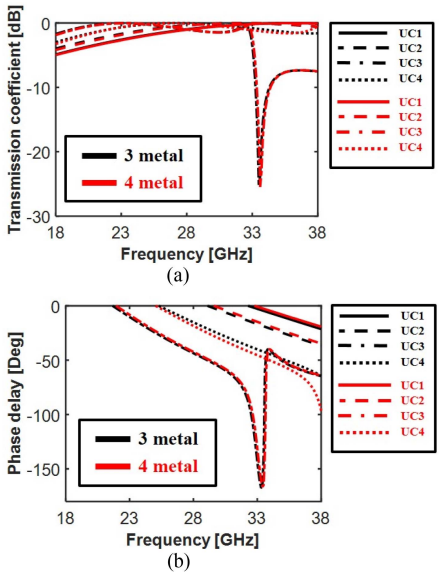

Fig. 3. Simulated results of the conventional unit cell with three metal layers and the proposed unit cells with four metal layers in the Ka-band. (a) Transmission coefficient. (b) Phase delay.

layers attached to both sides of the substrate. In Fig. 2(a), the unit cell based on a bandpass filter has two patches on layers 1 and 4 and two grids on layers 2 and 3 [13]. Fig. 2(b) shows the unit cell based on a low-pass filter that has only patches on all the layers [14], [15]. For the bandpass and low-pass unit cells, their dielectric constant, loss tangent, and the thickness of the substrates and the bondply are 2.98, 0.0013, and 127 μm, and 2.35, 0.0025, and 38 μm, respectively.

The grid and patch of the unit cells mean a shunt inductor and capacitor in terms of the equivalent circuit [14], [15]. The conventional unit cell with three metal layers has only three shunt components. However, the proposed unit cell has four metal layers so that one more shunt component can be added to the equivalent circuit. If the proposed unit cell is utilized at 28 GHz, the effect of the additional metal layer is negligible. Fig. 3 shows the transmission coefficient and the phase delay of the unit cells with three and four metal layers. Each transmission coefficient and phase delay of the unit cell with three or four metal layers are similar. As shown by the result in Fig. 3, the effect of an additional metal layer can be ignored. Because the thickness of the bondply between layers 2 and 3 is thin enough ($\approx 0.003\ \lambda_{0_{28\,\mathrm{GHz}}}$) compared to $\lambda_{0_{28\,\mathrm{GHz}}}$, the wavelength in the free space is at 28 GHz. However, an additional metal layer cannot be ignored because the thickness of the bondply is not negligible compared with the free-space wavelength at 140 GHz ($\approx 0.018\ \lambda_0$).

Fig. 4 illustrates the transmission coefficient and the phase delay of the unit cells with three metal layers at 140 GHz by varying the lengths of the patches (l_{1_x}, l_{1_y}, l_{2_x}, and l_{2_y}) and the width of the grids (w). The phase-shifting range is 208° at 140 GHz from $-248°$ to $-40°$ with a transmission coefficient less than -1.5 dB. Likewise, the transmission coefficient and the phase delay of the proposed unit cell are presented in Fig. 5, varying the lengths of the patches and the width of the grids. The proposed unit cells with a transmission coefficient less than -1.5 dB can achieve a phase-shift range of 271° from $-294°$ to

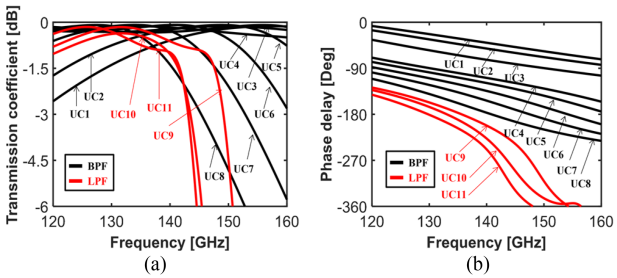

Fig. 4. Simulated results of the conventional unit cell with three metal layers in the *D*-band. (a) Transmission coefficient. (b) Phase delay.

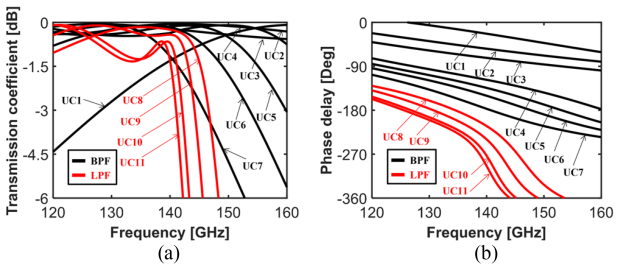

Fig. 5. Simulated results of the proposed unit cell with four metal layers in the *D*-band. (a) Transmission coefficient. (b) Phase delay.

TABLE I
GEOMETRIES OF THE PROPOSED UNIT CELL

Design	Cell	Dimensions (mm)
BPF in Fig. 5	UC1	W = 0.3, l_{1_x}= 0.1, l_{1_y}=0.1
	UC2	W = 0.2, l_{1_x}= 0.2, l_{1_y}=0.2
	UC3	W = 0.2, l_{1_x}= 0.3, l_{1_y}=0.3
	UC4	W = 0.3, l_{1_x}= 0.425, l_{1_y}=0.425
	UC5	W = 0.3, l_{1_x}= 0.45, l_{1_y}=0.45
	UC6	W = 0.3, l_{1_x}= 0.475, l_{1_y}=0.475
	UC7	W = 0.3, l_{1_x}= 0.5, l_{1_y}=0.5
LPF in Fig. 5	UC8	l_{1_x}= 0.5, l_{1_y}= 0.5, l_{2_x}= 0.525, l_{2_y}= 0.525
	UC9	l_{1_x}= 0.525, l_{1_y}= 0.525, l_{2_x}= 0.525, l_{2_y}= 0.525
	UC10	l_{1_x}= 0.55, l_{1_y}= 0.55, l_{2_x}= 0.525, l_{2_y}= 0.525
	UC11	l_{1_x}= 0.575, l_{1_y}= 0.55, l_{2_x}= 0.525, l_{2_y}= 0.525

−23°. The size and result of unit cells are shown in Table I and Table II, respectively.

III. TA PERFORMANCE ANALYSIS

A. TA and Feed Design

The distribution of the cells is determined using the ANSYS HFSS simulator based on the full-wave simulations. The wavefront radiated by the feed is focused on a given direction by compensating the required phase shift on the TA aperture. The required phase shifts must compensate for the difference in the spatial phase delay between the feed source and each unit cell.

The performance of the proposed unit cells was validated by designing a 224×224-element TA (this corresponds to a TA size of 94 λ_0×94 λ_0) to attain 45 dBi. The dimension of the TA aperture for which the spillover and tapered efficiency were maximized was determined.

TABLE II
PHASE DELAYS OF THE PROPOSED AND CONVENTIONAL UNIT CELL

	Fig. 4		Fig. 5	
Cell	Transmission coefficient (dB)	Phase delay (degree)	Transmission coefficient (dB)	Phase delay (degree)
UC1	−0.59	−40	−1.31	−23
UC2	−0.25	−51	−0.06	−54
UC3	−0.17	−73	−0.22	−73
UC4	−0.32	−109	−0.36	−118
UC5	−0.22	−119	−0.14	−134
UC6	−0.09	−134	−0.16	−150
UC7	−0.28	−153	−1.16	−177
UC8	−1.39	−177	−0.25	−212
UC9	−0.62	−202	−0.42	−240
UC10	−1.04	−227	−0.7	−273
UC11	−0.98	−248	−1.31	−294

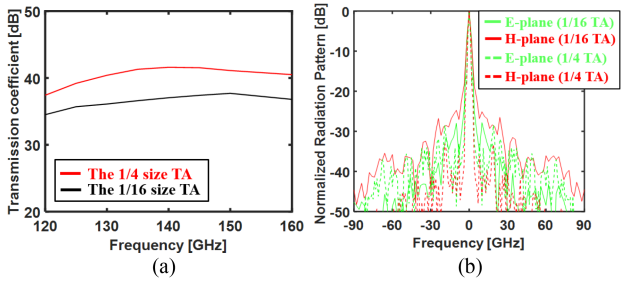

Fig. 6. Simulated results of the quarter size TA and 1/16 size TA. (a) Gain. (b) Normalized radiation pattern at 140 GHz under normal incidence.

A *D*-band horn antenna manufactured by RF-Lambda was used as the feeding source. The feed horn has a gain of 25.5 dBi at 140 GHz, and the half-power beamwidth of the source is 8.62° in the *E*-plane and 8.5° in the *H*-plane at 140 GHz. The focal length, *F* was set to 340 mm, and the focal-to-diameter (*F*/*D*) ratio was chosen as 1.687 to provide maximum aperture efficiency. The taper and spillover efficiency are dominant to the total efficiency. Utilizing the full-wave simulation, the taper and spillover efficiency were estimated to be 86% and 54%, respectively [16].

An effective simple medium [17] was adopted instead of unit cells to save time and to ensure that the gains of the large-size TAs are actually improved. The effective medium is the simple cuboid structure having constant permittivity and permeability. The effective medium has the same impedance as the air, and thus, the insertion loss becomes zero but produces various phase-shifting levels by varying the permittivity and permeability. In the design procedure, the phase-shifting levels of the effective medium-based unit cells were determined to be equal to the phase shifts of the actual FSS-based unit cells. Finally, this can reduce the required simulation resources and time dramatically.

To confirm the tendency of the TA gain and radiation pattern, the quarter and 1/16 size TA using an effective medium was simulated. Fig. 6 shows the simulated TA gain and radiation pattern of the quarter and 1/16 size TA with the effective medium.

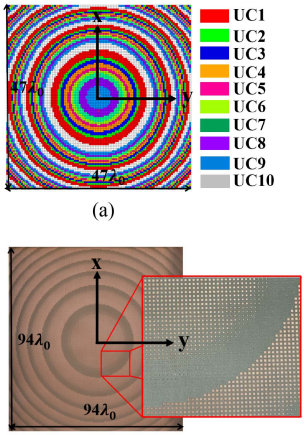

Fig. 7. (a) Cell distribution of the fabricated 112×112-element TA. (b) Proposed 224×224-element TA under normal incidence.

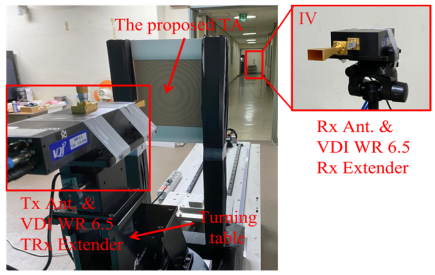

Fig. 8. Measurement setup with the simulated model in the HFSS.

Fig. 7(a) shows the cell distribution of the fabricated quarter-size TA consisting of 112×112-element. Fig. 7(b) shows the fabricated proposed TA consisting of 224×224-element.

B. Fabrication and Measurement

The proposed TA was fabricated using the standard PCB process. As stated above, the proposed TA consists of four metal layers, two substrates (Taconic NF-30), and one bonding layer (Tacbond 1.5). Fig. 7(b) shows a fabricated 224×224-element TA (this corresponds to a TA size of 94 λ_0×94 λ_0) using the proposed unit cells.

Fig. 8 presents the measurement setup of the proposed TA antenna that consists of an Anritsu MS4647B vector network analyzer, Tx, and Rx VDI WR 6.5 (110–170 GHz) waveguide extenders, and Rohde & Schwarz SMW200A vector signal generator. The proposed 224×224-element TA was illuminated by the *D*-band horn antenna located exactly at the center of the rotatable table. The distance between the receiver and transmitter was about 37 m to satisfy the far-field condition.

Fig. 9(a) presents the measured gain of the quarter-size TA and the proposed TA. Fig. 9(b) shows the results of the simulation and measured radiation pattern of quarter size TA. Fig. 9(c) and (d) presents the radiation pattern and cross-polarization of quarter size and the proposed TA, respectively. The gain and the radiation pattern of the quarter-size TA have a similar result to the simulation. The measured peak gain of quarter size TA and complete TA is 38.2 dBi and 44.3 dBi, respectively. The measured half-power beamwidth of the proposed TA at 140 GHz is 0.5° in the *E*-plane and 0.6° in the *H*-plane. The measured efficiency is 24.1%, and the measured bandwidth is 9 GHz (134.5–143.5 GHz).

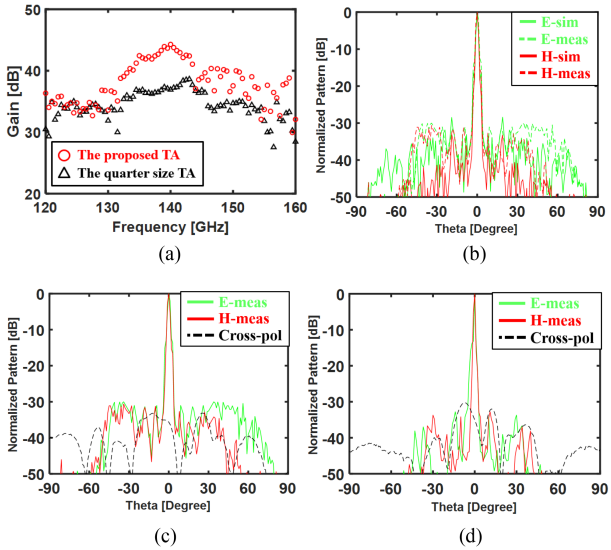

Fig. 9. Results of measurement. (a) Measured gain of the fabricated quarter size (112×112-element) and the proposed (224×224-element) TA under normal incidence. (b) Measured and simulated radiation pattern of the quarter size TA. (c) Measured radiation pattern of the quarter size TA. (d) Measured radiation pattern of the proposed TA.

TABLE III
COMPARISON OF THE PROPOSED TA WITH OTHER WORK IN THE *D*-BAND

Ref.	This letter	[18]	[19]	[20]
Freq (GHz)	140	140	145	150
Technology	PCB	LTCC	PCB	PCB
N. metal layers	4	7	3	3
Vias	No	Yes	Yes	No
Source gain (dBi)	25.5	20	10	19
Diameter	94λ	20λ	20λ	20λ
F/D	1.687	1.87	0.75	0.75
Peak gain (dBi)	44.29	33.5	33.0	32
3 dB Bandwidth	6.4%	24.4%	19.8%	19.8%
Max. aperture efficiency	24.1%	50.1%	38.3%	32%

IV. CONCLUSION

This letter presents a low-profile and high-gain TA in the *D*-band fabricated using the standard PCB process. It should be noted that the TA in previous works could not attain a peak gain above 40 dBi in the sub-THz. A novel scheme is presented to overcome the limitation of the PCB fabricated conventional unit cells by FSS enhancement of the phase-shift range in the *D*-band. The proposed TA was compared with the previously developed TA. The tunable range with less than a 1.5 dB insertion loss is as much as wide, and a peak gain of 44.29 dBi is attained. These results suggest that, in the future, the improvement of the RF performance of the TA will enable 6G communication technologies to be implemented. The comparison of transmitarrays in *D*-band is presented in Table III. This letter demonstrates that a novel and efficient unit cell scheme can overcome the limitation of the PCB process and enhance the inherent performance in the *D*-band.

REFERENCES

[1] F. Xu et al., "Big data driven mobile traffic understanding and forecasting: A time series approach," *IEEE Trans. Serv. Comput.*, vol. 9, no. 5, pp. 796–805, Sep./Oct., 2016.

[2] H.-J. Song and T. Nagatsuma, "Present and future of terahertz communications," *IEEE Trans. Terahertz Sci. Technol.*, vol. 1, no. 1, pp. 256–263, Sep. 2011.

[3] T. Nagatsuma, "Advances in terahertz communications accelerated by photonics technologies," in *Proc. 24th Optoelectron. Commun. Conf. Int. Conf. Photon. Switching Comput.*, 2019, pp. 1–3.

[4] K. Rikkinen, P. Kyosti, M. E. Leinonen, M. Berg, and A. Parssinen, "THz radio communication: Link budget analysis toward 6G," *IEEE Commun. Mag.*, vol. 58, no. 11, pp. 22–27, Nov. 2020.

[5] Y. He, Y. Chen, L. Zhang, S.-W. Wong, and Z. N. Chen, "An overview of terahertz antennas," *China Commun.*, vol. 17, no. 7, pp. 124–165, Jul. 2020.

[6] I. A. Hemadeh, K. Satyanarayana, M. El-Hajjar, and L. Hanzo, "Millimeter-wave communications: Physical channel models, design considerations, antenna constructions, and link-budget," *IEEE Commun. Surv. Tuts.*, vol. 20, no. 2, pp. 870–913, Apr./Jun. 2018.

[7] M. Marcus and B. Pattan, "Millimeter wave propagation: Spectrum management implications," *IEEE Microw. Mag.*, vol. 6, no. 2, pp. 54–62, Jun. 2005.

[8] F. Giannetti, M. Luise, and R. Reggiannini, "Mobile and personal communications in the 60 GHz band: A survey," *Wireless Pers. Commun., Int. J.*, vol. 10, no. 2, pp. 207–243, 1999.

[9] P. Pietraski, D. Britz, A. Roy, R. Pragada, and G. Charlton, "Millimeter wave and terahertz communications: Feasibility and challenges," *ZTE Commun.*, vol. 10, no. 4, pp. 3–12, Dec. 2012.

[10] N. Behdad, M. Al-Joumayly, and M. Salehi, "A low-profile third-order bandpass frequency selective surface," *IEEE Trans. Antennas Propag.*, vol. 57, no. 2, pp. 460–466, Feb. 2009.

[11] M. Salehi and N. Behdad, "A second-order dual X-/Ka-band frequency selective surface," *IEEE Microw. Wireless Compon. Lett.*, vol. 18, no. 12, pp. 785–787, Dec. 2008.

[12] M. Al-Joumayly and N. Behdad, "A new technique for design of low-profile, second-order, bandpass frequency selective surfaces," *IEEE Trans. Antennas Propag.*, vol. 57, no. 2, pp. 452–459, Feb. 2009.

[13] N. Behdad and M. A. Al-Joumayly, "A generalized synthesis procedure for low-profile, frequency selective surfaces with odd-order bandpass responses," *IEEE Trans. Antennas Propag.*, vol. 58, no. 7, pp. 2460–2464, Jul. 2010.

[14] J. Oh, "Millimeter-wave thin lens employing mixed-order elliptic filter arrays," *IEEE Trans. Antennas Propag.*, vol. 64, no. 7, pp. 3222–3227, Jul. 2016.

[15] J. Oh, "Millimeter-wave short-focus thin lens employing disparate filter arrays," *IEEE Antennas Wireless Propag. Lett.*, vol. 15, pp. 1446–1449, 2016, doi: 10.1109/LAWP.2015.2512853.

[16] A. Yu, F. Yang, A. Z. Elsherbeni, J. Huang, and Y. Rahmat-Samii, "Aperture efficiency analysis of reflectarray antennas," *Microw., Opt. Technol. Lett.*, vol. 52, pp. 364–372, 2010, doi: 10.1002/mop.24949.

[17] Y. Kim, H. Kim, I. Yoon, and J. Oh, "4 × 8 patch array-fed FR4-based transmit array antennas for affordable and reliable 5G beam steering," *IEEE Access*, vol. 7, pp. 88881–88893, 2019, doi: 10.1109/ACCESS.2019.2926379.

[18] Z.-W. Miao et al., "140 GHz high-gain LTCC-integrated transmit-array antenna using a wideband SIW aperture-coupling phase delay structure," *IEEE Trans. Antennas Propag.*, vol. 66, no. 1, pp. 182–190, Jan. 2018, doi: 10.1109/TAP.2017.2776345.

[19] F. Foglia Manzillo, A. Clemente, and J. L. González-Jiménez, "High-gain D-band transmitarrays in standard PCB technology for beyond-5G communications," *IEEE Trans. Antennas Propag.*, vol. 68, no. 1, pp. 587–592, Jan. 2020, doi: 10.1109/TAP.2019.2938630.

[20] W. Saleh, Y. Letestu, R. Sauleau, and E. M. Cruz, "Design and measurements of a high-performance wideband transmitarray antenna for D-band communications," *IEEE Antennas Wireless Propag. Lett.*, vol. 20, no. 9, pp. 1765–1769, Sep. 2021, doi: 10.1109/LAWP.2021.3096743.